

JOURNAL OF MECHANICS OF CONTINUA AND MATHEMATICAL SCIENCES www.journalimcms.org



ISSN (Online): 2454 -7190 Vol.-20, No.-11, November (2025) pp 20-29 ISSN (Print) 0973-8975

IMPACT OF PLATE THICKNESS ON 3D TEMPERATURE DISTRIBUTION IN WELDING: FINITE DIFFERENCE METHOD APPROACH

Adak M1. and Mandal A2

¹Dept of Applied Maths. and Hum, YCCE, Nagpur, India-441110.

²Department of Civil Engineering, VNIT, Nagpur, India-440010.

Email: 1 malabikaadak7@gmail.com, 2 amandalthesis@yahoo.com

Corresponding Author: Adak M.

https://doi.org/10.26782/jmcms.2025.11.00002

(Received: August 14, 2025; Revised: October 11, 2025; October 27, 2025)

Abstract

This study examines the impact of plate thickness on three-dimensional temperature distribution during welding, employing the finite difference method for computational modeling. The analysis highlights how variations in thickness affect temperature profiles within welded structures. Key focus areas include the development of heat transfer equations, boundary condition handling, and the integration of welding parameters and material properties. Model validation against experimental data confirms its accuracy and adaptability to diverse welding scenarios. The findings enhance understanding of thermal dynamics, contributing to improved weld quality, reduced defects, and optimized welding efficiency.

Keywords: Finite Difference Method, Plate Thickness, Temperature Distribution, Welding Process.

Nomenclature

- c mass-specific heat, J/kgK
- q volumetric density of the heat source, kg/mm³
- h convection coefficient, W/mm²K.
- V Voltage, Volt
- I Current, ampere
- Q thermal energy input per unit of volume
- T Temperature, K
- T₀ Initial Temperature, K

Greek Symbols

- ρ material density, kg/mm³
- η arc coefficient factor
- λ_x Thermal conductivity along x axis, W/(mm·K)

- $\lambda_{\rm v}$ Thermal conductivity along x axis, W/(mm·K)
- λ_z Thermal conductivity along x axis, W/(mm·K)

I. Introduction

Welding is a fundamental manufacturing process used extensively in structural, mechanical, and aerospace engineering applications. The quality and performance of a welded joint are significantly influenced by the thermal behavior that occurs during the welding process. Among the various factors affecting heat transfer during welding, plate thickness plays a crucial role. Analytical solutions to threedimensional heat conduction problems are often impractical due to nonlinear boundary conditions and transient heat sources. The finite difference method (FDM) offers a robust and straightforward approach for discretizing and solving the governing heat transfer equations. Through this method, temperature distributions can be computed at discrete spatial and temporal points, providing detailed insights into transient thermal behavior. Numerical modeling, especially the finite difference method (FDM), enables precise 3D temperature prediction for process optimization. Early work by Rosenthal [XXI] provided exact solutions for heat transfer, followed by significant contributions in finite element thermal simulations from researchers such as Kamala and Goldak [XIV], Nguyen et al. [XIX], Tekriwal and Mazumder [XXIV], Bonifaz [VIII], and Yeung and Thornton [XXVI]. Reviews by Liu and David [XVI] and Saha and Pal [XXII] outline modeling techniques, while Patankar [XX] provides foundational theory for the finite difference method. Advanced multi-physics approaches and calibration studies [X, XI, XII, XIII, XXV] and studies by Adak et al. [I-VII] expanded FDM applications, with analytical solutions also explored [XVII, XVIII, XXII]. This survey examines research on FDM-based models for predicting three-dimensional temperature distribution in welding with convection boundaries, developing and validating a model that integrates welding parameters, material properties, and heat source characteristics to improve weld quality, reduce defects, and enhance efficiency.

II. Mathematical Model

The focus of this study lies on thermal modeling and simulation, particularly emphasizing heat source modeling. Presented herein are simulation outcomes pertaining to submerged arc welding. The fundamental equation governing heat transfer within the weld region is the equation governing heat conduction, which defines how heat changes over time and space due to thermal gradients. In its general form, the equation governing heat conduction is given by

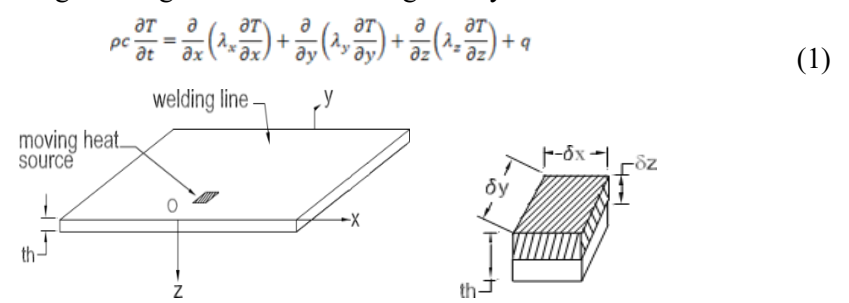


Fig.1. Configuration of system of axes and the volumetric model for the source of heat

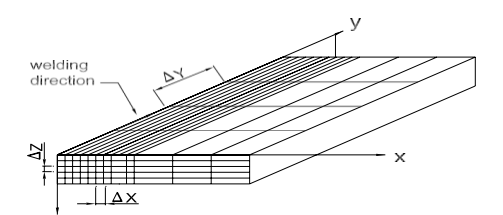


Fig. 2. Finer and coarser mesh structures for the numerical analysis

Figure 1 shows the coordinate system and volumetric heat source model, with heating along the y-axis and a fine 1 mm grid in the x and z directions. After the initial transient phase, a coarser mesh—matching torch speed—is used along y. Since the heating axis is centered, only half the plate around the y-axis is modeled (Figure 2 [XV]). The arc efficiency factor η , accounting for various heat losses, is set to 0.9 [25]. As a result, the heat delivered to the plate is expressed as η VI. This heat is assumed to be evenly distributed over the shaded region of the model of source heat, as depicted in Figure 1 [XV]. Accordingly, the thermal energy input per unit of volume is given by $Q = \frac{\eta VI}{dxdydz}$

Boundary Conditions

The boundary condition along y-axis (heat source passes through y-axis) is

$$\frac{\partial T}{\partial x} = 0$$

Convection will facilitate heat dissipation along the three borders except the heat line and on the upper and lower surfaces of the plate. As a result, specific boundary conditions are outlined for these surfaces.

Boundary condition along the edge of the plate parallel to y-axis,

$$\lambda_x \frac{\partial T}{\partial x} + h(T(x, y, z) - T_0) = 0$$

Boundary condition along the edge of the plate in the direction of x-axis,

$$\lambda_y \frac{\partial T}{\partial y} + h(T(x, 0, z) - T_0) = 0$$

Boundary condition along the edge of the plate parallel to x-axis,

$$\lambda_{y} \frac{\partial T}{\partial y} + h(T(x, y, z) - T_{0}) = 0$$

Boundary condition along the upper surface of the plate in the direction of z-axis.

$$\lambda_z \frac{\partial T}{\partial z} + h(T(x, y, 0) - T_0) = 0$$

Boundary condition along the lower surface of the plate parallel to z axis.

$$\lambda_z \frac{\partial T}{\partial z} + h(T(x, y, z) - T_0) = 0$$

Convection Coefficient

The model applies Newton's convection cooling, $q = h(T - T_0)$ with temperature-dependent coefficients (Table 1 [26]). During welding $h = 4.5 \times 10^{-4}$ is used within 50 mm of the weld line on the upper surface, and $h = 1.8 \times 10^{-5}$ for the cooler remaining plate area.

Table 1: Convection coefficient dependent on temperature for steel structure

$(\mathbf{T}-\mathbf{T}_0) [\mathbf{K}]$	h [W/mm ² K]			
0	0			
55	1.8154 × 10–6			
277	9.0795 × 10–6			
555	1.8156 × 10-5			
2777	5.2666 × 10-5			
3777	$1.0895 \times 10 - 3$			

Material Properties

Steel's thermal and mechanical properties vary greatly with temperature, and accurate high-temperature data are difficult to obtain. Combined with modeling assumptions, property calculations remain approximations. Thermal history is computed considering temperature-dependent specific heat and thermal conductivity [27], as shown in Table 2.

Table 2: Temperature-dependent specific heat and thermal conductivity of *C-Mn* steel

	T(K)	293	373	573	773	973	1073	1273	1473	1673	> 1673
λ	(J/mmsK)	0.0548	0.0526	0.0455	0.0393	0.0324	0.0255	0.0278	0.0291	0.0313	0.0422
	C (J/kgK)	397	435	546	686	894	928	679	739	799	400

III. Solution Procedure

FDM involves replacing the derivatives in a differential equation (DE) with an approximately equivalent finite difference equation. The solution process follows these steps:

- (i) The solution domain is discretized by dividing it into small rectangles using a mesh and nodes.
- (ii) The given DE is approximated by equivalent finite difference equations that provide solutions at each mesh point.
- (iii) Apply the initial and boundary conditions to generate a system of simultaneous equations.
- (iv) The Gauss-Seidel method is used to solve the system of equations.

By applying the forward difference for the first-order derivative and the central difference approximation for the second-order derivative, equation (1) is replaced by:

$$\begin{split} \frac{\partial^2 T}{\partial x^2} &= \frac{T^n{}_{i+1} - 2T^n_i + T^n_{i-1}}{(\Delta x)^2} + O(\Delta x^2) \\ \frac{\partial^2 T}{\partial y^2} &= \frac{T^n{}_{j+1} - 2T^n_j + T^n_{j-1}}{(\Delta y)^2} + O(\Delta y^2) \\ \frac{\partial^2 T}{\partial z^2} &= \frac{T^n{}_{k+1} - 2T^n_k + T^n_{k-1}}{(\Delta z)^2} + O(\Delta z^2) \end{split}$$

The O() terms denote the method's local truncation error, which is negligible here, allowing derivation of the difference equations. The heat equation was solved using a finite difference central explicit scheme ($\lambda \le 1/2$) with fine grids and small time steps, and a Jacobi iteration with under-relaxation for stability and temperature-dependent properties. The code was written in C.

IV. Results and Discussion

The model used mesh systems of $132 \times 32 \times 8$, $132 \times 32 \times 10$, $132 \times 32 \times 12$, and $132 \times 32 \times 14$ for 6, 8, 10, and 12 mm plates, respectively, computing temperature profiles over 1500 steps of 0.2 s each. The heat conduction equation, with given material properties, was solved using welding parameters of 380 A, 36 V, and 8 mm/s. Figures 3–5 show temperature evolution, contour plots, and fusion/HAZ zones, revealing that thicker plates dissipate more heat, reducing fusion depth and increasing cooling rates.

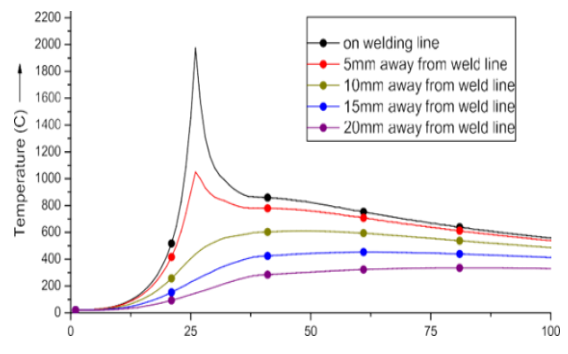


Fig. 3. Transient temperature distribution on the top surface of a 6 mm plate

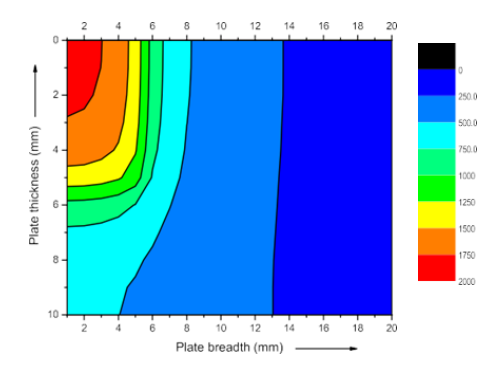


Fig. 4. Contour plot along the xz plane for a 10 mm plate

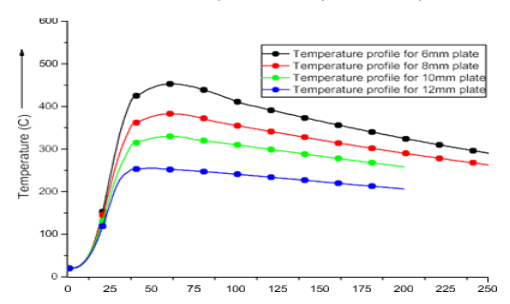


Fig. 5. Variation of temperature profiles with plate thickness

Experimental Verification

To validate the numerical model of heat flow analysis, multiple bead-on-plate welding experiments were conducted on C-Mn steel test specimens of four varying thicknesses. The welding parameters are given previously. Submerged arc welding was employed, as illustrated in Figure 6. The chemical composition of the flux and filler metal was assessed using the ZAF quantitative method of scanning electron microscopy, with system resolutions of 67 and 68, respectively. The compositions are given in Table 3.

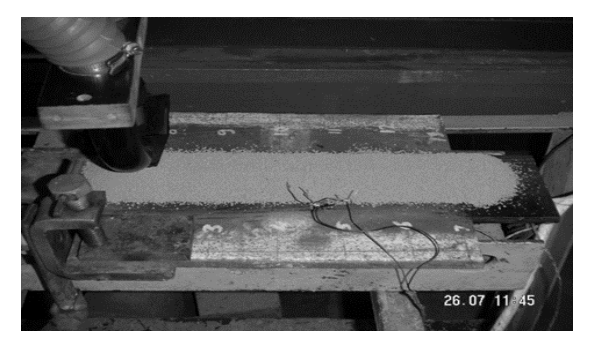


Fig. 6. Setup for Submerged arc welding (SAW)

Table 3: Qualitative Analysis of Flux and Filler Wire used in Welding (SAW)

Analysis of f	iller wire	Analysis of flux			
Element	%	Compound	%		
C	0.19	Sio ₂	31.23		
Si	0.34	TiO_2	1.02		
Mn	0.44	MgO	17.43		
Cu	0.06	CaO	20.65		
Al	0.05	InAs	1.78		
P	less than 0.02	Fe_2O_3	3.26		
S	less than 0.02	Al_2O_3	21.44		
		MnO	3.18		

To measure the temperature distribution, thermocouples were employed on both the upper and lower surfaces of the four distinct plates during welding, as depicted in Figure 7. Chromel-alumel K-type thermocouples were utilized to collect temperature data. The voltage signals from the thermocouples were directly connected to an Agilent

34970A Data Acquisition system, which was interfaced with a computer. Temperature readings were recorded at one-second intervals. Welding operations were conducted using direct current electrode positive polarity, with the contact tube to workpiece distance maintained at 25 mm.

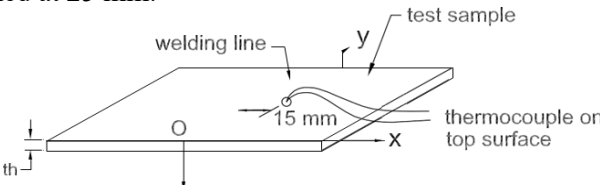


Fig. 7. Thermocouple locations for temperature measurement

In all welding instances, thermocouples were utilized to capture the temperature evolution on both the top and bottom surfaces of the plates. However, in certain instances, they failed to register the temperature accurately. The recorded temperature histories were then compared with the calculated ones. Sample results and the percentage deviations for the peak temperature are presented in Table 4.

Table 4: Weld parameters, experimental and calculated peck temperatures at a point 15 mm away from weld line

Sl.	Plate	Welding Par		ameters	Peck Temperature		
No.	Thk	Current	Voltage	Speed	Cal.	Exp.	%Dev.
	(mm)	(A)	(V)	(mm/s)	(0C)		
1	6	400	30	11	405	399	2.50
2	8	380	30	9	426	436	2.29
3	10	420	28	12	290	289	0.35
4	12	360	28	10	257	260	1.15

A total of 76 test samples consisting of mild steel plates with thicknesses of 6 mm, 8 mm, 10 mm, and 12 mm were employed in the experiments. The maximum deviation observed for the peak temperature at a point 15 mm away from the weld line was below 3%. This demonstrates the repeatability of the experiments and thus ensures the replicability of the comparisons. The temperature profiles obtained through numerical simulation at the thermocouple locations are illustrated in Figures 8 and 9. These figures indicate a close agreement between the numerical temperature distributions and those obtained experimentally, thereby validating the numerical model for heat flow analysis.

Experimental temperature profile
Numerical temperature profile
200
300
0 50 100 150 200 250 300

Fig. 8. Temperature profile 15 mm away from the weld line on the bottom surface of an 8 mm plate

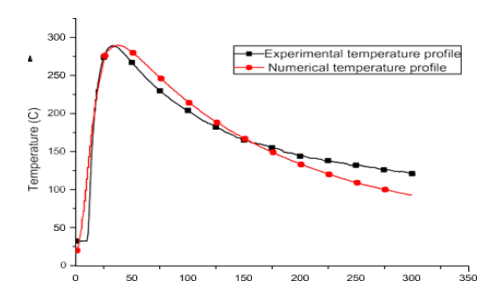


Fig. 9. Temperature profile 15 mm away from the weld line on the top surface of a 12 mm plate

V. Conclusions

This dissertation develops and validates a theoretical heat flow model for welding, using bead-on-plate submerged arc welding on 6–12 mm C-Mn steel plates. An explicit central difference method with a volumetric heat source was used to simulate the transient 3D thermal cycle, incorporating convection boundaries and temperature-dependent properties. Numerical results matched experiments within 3%, accurately predicting temperature distribution and weld zones. Thicker plates exhibited faster cooling rates, which increased the risk of hydrogen embrittlement but stabilized sooner. The model proves robust for welding optimization and material control.

Conflict of Interest:

There was no relevant conflict of interest regarding this paper.

References

- Adak M. and Mandal N.R (2009), Pseudolinear equivalent constant rigidity concept for analyzing welding residual deformation, Applied Mathematical Modelling 33, 2096–2108. 10.1016/j.apm.2008.05.024.
- II. Adak M. and Mandal N.R (2010), Numerical and experimental study of mitigation of welding distortion, Applied Mathematical Modelling 34, 146–158. 10.1016/j.apm.2009.03.035.
- III. Adak M. and Soares Guedes C. (2014), Effects of different restraints on the weld-induced residual deformations and stresses in a steel plate, International Journal of Advanced Manufacturing Technology, 71, 699–710. 10.1007/s00170-013-5521-9.
- IV. Adak M. (2020), "Comparison of Explicit and Implicit Finite difference Schemes on Diffusion Equation", In book: Mathematical Modeling and Computational Tools, 227-238. 10.1007/978-981-15-3615-1 15.

- J. Mech. Cont. & Math. Sci., Vol.-20, No.-11, November (2025) pp 20-29
- V. Adak M. and A. Mandal, "Numerical Solution of 2nd Order Boundary Value problems with Dirichlet, Neumann and Robin Boundary Conditions using FDM", Communication in Mathematics and Application, Vol. 13, Issue.2, page 529-537, 2022. 10.1088/1742-6596/2070/1/012052.
- VI. Adak M., "Numerical Solution of Laplace and Poisson Equations for Regular and Irregular Domain Using Five-Point Formula", Book: Applied Analysis, Computation and Mathematical Modelling in Engineering. 10.1007/978-981-19-1824-7, 2022.
- VII. Adak M., A Mandal and A. Meshram, "Explicit Finite Difference Approach on Multi-Dimensional Wave Equation with Constant Propagation", Taylor and Frances group, Recent Advances in Material, Manufacturing and Machine Learning, ISBN 9781003450252, 2024. 10.1201/9781003450252.
- VIII. Bonifaz E (2000) Finite element analysis of heat flow in single pass arc welds. Welding Research Supplement 2: 121-125.
 https://www.researchgate.net/publication/275022082_
 Finite Element Analysis of heat flow in single pass arc welds.
- IX. DebRoy, T. (2018). Science of friction stir welding and processing. Science, 368(6493), a2588.
- X. Dong, P., Hong, J. K., & Rogers, P. (1998). Analysis of residual stresses in Al–Li repair welds and mitigation techniques. Welding Journal, 439s–445s. https://www.osti.gov/biblio/292961.
- XI. Grong, Ø. (1994). Metallurgical Modeling of Welding. The Institute of Materials, Cambridge.
- XII. Gundersen, Ø., & Zhang, Z. (1999). Modeling of residual stresses in weld simulated restrained C–Mn steel specimens. In Proceedings of the Ninth International Offshore and Polar Engineering Conference, Brest, France, May 30–June 4, pp. 187–194.
- XIII. Haidar, J., & David, S. A. (2016). Calibration and validation of welding simulations. Welding Journal, 95(3), 77s–85s.
- XIV. Kamala, V., & Goldak, J. (1993). Error due to two-dimensional approximation in heat transfer analysis of welds. Welding Journal, September, 2, 440–446.
- XV. Kumar, A., & Muthukrishnan, N. (2019). Influence of welding parameters on temperature distribution in gas tungsten arc welding of AA6061 alloy using numerical simulation. Materials Today: Proceedings, 15, 1782–1789.
- XVI. Liu, S., & David, S. A. (2017). A review of three-dimensional finite element modeling of welding processes. Journal of Manufacturing Science and Engineering, 139(10), 100801.

- J. Mech. Cont. & Math. Sci., Vol.-20, No.-11, November (2025) pp 20-29
- XVII. Mohammad, B. N., & Norbert, E. (2019a). An analytical solution for temperature distribution in fillet arc welding based on an adaptive function. Welding in the World, 63, 409–419. 10.1007/s40194-018-0667-6
- XVIII. Mohammad, B. N., & Norbert, E. (2019b). Powerful analytical solution to heat flow problem in welding. International Journal of Thermal Sciences, 135, 601–612. 10.1016/j.ijthermalsci.2018.08.003
- XIX. Nguyen, N., Ohta, A., Matsouka, K., Suzuki, N., & Maeda, Y. (1999). Analytical solutions for transient temperature of semi-infinite body subjected to 3D moving heat sources. Welding Journal, August, 9, 265–274.
- XX. Patankar, S. V. (2018). Numerical Heat Transfer and Fluid Flow. CRC Press.
- XXI. Rosenthal, D. (1946). The theory of moving sources of heat and its application to metal treatments. Transactions of ASME, 2, 849–866.
- XXII. Saha, P., & Pal, S. K. (2015). Analysis of temperature distribution in gas metal arc welding process using finite difference method. Journal of Manufacturing Processes, 18, 65–74.
- XXIII. Suresh, K. K. (2014). Analytical modeling of temperature distribution, peak temperature, cooling rate and thermal cycles in a solid work piece welded by laser welding process. Procedia Materials Science, 6, 821–834. 10.1016/j.mspro.2014.07.099
- XXIV. Tekriwal, P., & Mazumder, J. (1988). Finite element analysis of three-dimensional transient heat transfer in GMA welding. Welding Research Supplement, 2, 150–156.
- XXV. Thi-Thao Ngo, Chi-Chang Wang, Jin H. Huang, & Van-The Than (2019). Estimating heat generation and welding temperature for gas metal arc welding process. Applied Thermal Engineering, 160, 114056. 10.1016/j.applthermaleng.2019.114056.
- XXVI. Yeung, K., & Thornton, P. (1999). Transient thermal analysis of spotwelding electrodes. Welding Research Supplement. chrome-extension://efaidnbmnnnibpcajpcglclefindmkaj/https://s3.us-east-1.amazonaws.com/WJ www.aws.org/supplement/WJ_1999_01_s1.pdf.
- XXVII. Zhang, L., & Zhang, Y. (2018). Advanced numerical modeling and simulation of resistance spot welding: A review. International Journal of Heat and Mass Transfer, 118, 964–994.